

Prospects of searches for long-lived charged particles with MoEDAL

B.S. Acharya^{a,b}, A. De Roeck^{c,d}, J. Ellis^{b,e,f}, D.K. Ghosh^g, R. Masełek^h, G. Panizzo^{a,i}, J.L. Pinfold^j, K. Sakurai^h, A. Shaa^h, A. Wall^k

^aThe Abdus Salam International Centre for Theoretical Physics, Strada Costiera 11, Trieste, Italy

^bTheoretical Particle Physics and Cosmology Group, Department of Physics, King's College London, Strand, London WC2R 2LS, UK

^cExperimental Physics Department, CERN, CH1211 Geneva 23, Switzerland

^dAntwerp University, B2610 Wilrijk, Belgium

^eTheoretical Physics Department, CERN, CH1211 Geneva 23, Switzerland

^fNational Institute of Chemical Physics & Biophysics, R avala 10, 10143 Tallinn, Estonia

^gSchool of Physical Sciences, Indian Association for the Cultivation of Science, 2A & 2B Raja S.C. Mullick Road, Kolkata 700 032, India

^hInstitute of Theoretical Physics, Faculty of Physics, University of Warsaw, ul. Pasteura 5, PL-02-093 Warsaw, Poland

ⁱINFN Gruppo Collegato di Udine, Sezione di Trieste, Udine

^jPhysics Department, University of Alberta, Edmonton, Alberta T6G 2E4, Canada

^kUniversity of Alabama, Department of Physics, Tuscaloosa, Alabama, USA

Abstract

We study the prospects of searches for exotic long-lived particles with the MoEDAL detector at the LHC, assuming the integrated luminosity of 30 fb^{-1} that is expected at the end of Run 3. MoEDAL incorporates nuclear track detectors deployed a few metres away from the interaction point, which are sensitive to any highly-ionizing particles. Hence MoEDAL is able to detect singly- or doubly-charged particles with low velocities $\beta < 0.15$ or < 0.3 , respectively, and lifetimes larger than $\mathcal{O}(1) \text{ m}/c$. We examine the MoEDAL sensitivity to various singly-charged supersymmetric particles with long lifetimes and to several types of doubly-charged long-lived particles with different spins and SU(2) charges. We compare the prospective MoEDAL mass reaches to current limits from ATLAS and CMS, which involve auxiliary analysis assumptions. MoEDAL searches for doubly-charged fermions are particularly competitive.

1. Introduction

One of the key priorities of the LHC experimental programme is to search for new particles beyond the Standard Model, or at least set robust constraints on their possible existence. Priorities during Runs 1 and 2 of the LHC included scans for bumps in invariant-mass spectra, searches for excesses of missing transverse energy in events with various topologies, and precision tests of Standard Model (SM) predictions. With the striking exception of the discovery of the Higgs boson, none of these searches has yet borne any fruit.

In parallel with these mainstream searches for new particles, there has been growing interest in less-orthodox searches. These have included searches for long-lived particles (LLPs), which we review in Section 2. These long-lived particles may arise in various scenarios beyond the SM that satisfy any of the following conditions: (i) small couplings, (ii) nearly degenerate masses or (iii) heavy intermediate (virtual) particles mediating decays [1–3]. We expect such searches to receive increased attention during LHC Run 3.

During Runs 1 and 2 of the LHC the search for magnetically-charged particles was the main objective of the MoEDAL experiment, which has published limits from searches for magnetic monopoles [4] and dyons [5]. The ATLAS Collaboration has also published limits on magnetic monopole production [6].

As we discuss in Section 3 one of the key features of the MoEDAL detector [7] is its array of panels of nuclear track detectors (NTDs), which can register anomalously heavy ionization as would be produced by singly-charged particles with velocities $\beta \equiv v/c < 0.15$, or by doubly-charged particles with $\beta < 0.3$. The MoEDAL NTD panels are located at distances ~ 2 m from the interaction point, and are therefore sensitive to long-lived heavily-ionizing particles with lifetimes τ longer than $\mathcal{O}(1)$ m/c [8, 9]. We discuss in Section 4 the analysis framework that we use to study long-lived charged particles, which we apply to a couple of well-motivated theoretic models in Sections 5 and 6.

One such model is supersymmetry, which has

been the object of many other searches at the LHC [10, 11]. The minimal supersymmetric extension of the SM (the MSSM) does not contain any doubly-charged particles, but many of its singly-charged particles are candidates to be long-lived, and several mechanisms suggest this possibility [12–15]. The lightest supersymmetric particle (LSP) would be stable if R-parity is conserved, but could be unstable with a long lifetime if R-parity is weakly broken [16, 17]. Even if R-parity is conserved, the next-to-lightest supersymmetric particle (NLSP) could be long-lived if it is very nearly degenerate with the LSP, as in coannihilation scenarios, or if the supersymmetric particle(s) mediating its decay is (are) very heavy, as in scenarios with split supersymmetry [18, 19]. Another possibility is that the LSP has only very weak interactions, e.g., if it is the gravitino or some other particle with gravitational-strength interactions, or if it is located in a well-sequestered hidden sector. In either case, the lightest supersymmetric particle in the visible sector could be long-lived [20–22].

Prospects for discovering long-lived sparticles with MoEDAL was first discussed in [8, 9]. These studies considered a double long-lived (LL) cascade chain: $pp \rightarrow \tilde{g}\tilde{g}$, $\tilde{g} \rightarrow jj[\tilde{\chi}_1^0]_{\text{LL}}$, $[\tilde{\chi}_1^0]_{\text{LL}} \rightarrow \tau[\tilde{\tau}]_{\text{LL}}$, assuming that the $\tilde{\chi}_1^0$ and $\tilde{\tau}$ are both long-lived. In this paper we extend this discussion to consider direct pair production of general meta-stable sparticles, including charged R-hadrons containing a gluino, squark or stop, as well as Winos, Higgsinos and sleptons, without making any specific assumptions about the models in which they appear [23].

A second scenario that may lead to a long-lived heavy fermion is a Type-III seesaw model [24–26], in which the SM is augmented with at least two $SU(2)_L$ -triplet fermion fields (Σ) with $Y = 0$. The observed neutrino mass is given by $m_\nu \approx Y_\nu^2 v^2 / m_\Sigma$, where Y_ν is the Dirac Yukawa coupling, v is the SM vev and m_Σ is the mass of the heavy triplet fermion. In this model, radiative corrections generate a mass splitting $m_{\Sigma^\pm} - m_{\Sigma^0} > m_\pi^\pm$ [27, 28] so that the decay $\Sigma^\pm \rightarrow \Sigma^0 + \pi^\pm$ is kinematically allowed, with a lifetime $\mathcal{O}(10^{-8})$ s that leads to very soft charged pion but no long-lived charged-particle track. How-

ever, if there are additional contributions to the $\Sigma^{\pm,0}$ masses that reduce the mass difference so that the two-body decay is not allowed, the dominant decay of the Σ^{\pm} would be three-body with a lifetime $\mathcal{O}(10^{-6})$ s. The latter case would lead to a detectable long-lived charged particle signature similar to that of the Wino, as we discuss later in the paper.

A long-lived doubly-charged scalar particle may appear in a number of models. One example is a Type-II seesaw model of neutrino masses, in which the SM is supplemented by a complex $SU(2)_L$ triplet of scalar fields with hypercharge $Y = 2$ [29–37], and other scenarios for doubly-charged scalars are mentioned later. Another possibility for a doubly-charged particle is a spin-1/2 particle, such as a doubly-charged Higgsino as appears in supersymmetric L-R models [38–42]. One can also simply add doubly-charged scalars and fermions in various $SU(2)_L$ representations to the particle content of the SM, then write down the SM gauge-invariant interaction terms involving these new fields and study their phenomenology [43, 44]. We consider here doubly-charged particles that may be scalars or fermions and either singlets or triplets of the SM $SU(2)_L$ gauge group, without making any specific assumptions about the models in which they appear.¹

Both ATLAS [49, 50] and CMS [51] have set limits on certain species of long-lived supersymmetric particles, ATLAS has also considered multi-charged particles [52], and CMS [51] has also considered one example of a doubly-charged fermion as well as multi-charged particles [53], as we review in Section 2. However, the ATLAS and CMS searches both employed auxiliary signatures, in particular either E_T^{miss} or muon triggers [1–3]. Not all models containing long-lived charged particles would yield a large E_T^{miss} signature, and therefore the data sets used are a combination of both these complementary triggers, so as to reduce substantially the model dependence of the search. The MoEDAL analysis would not invoke any such a signatures, and hence is fully model-independent. In Table 1 we compare the

prospective sensitivities of MoEDAL for a wide selection of supersymmetric candidates with the results of ATLAS and CMS, and Table 2 shows a similar comparison for a wide selection of doubly-charged candidates.

We note in passing that the parameter spaces of both the Type-II and-III seesaw models, as well as L-R symmetric models, are constrained by various theoretical considerations and low-energy experimental data [35–37, 45, 46, 54]. Since our goal in this paper is to estimate the MoEDAL sensitivities on these exotic particles in a model-independent way, we refrain from discussing further these indirect model-dependent limits.

The outline of our paper is as follows. In Section 2 we review previous searches for long-lived charged particles at the LHC by ATLAS and CMS. Then, in Section 3 we review relevant aspects of the MoEDAL detector, and in Section 4 we describe the analysis framework we use. The prospective sensitivities of MoEDAL for long-lived supersymmetric particles are obtained in Section 5 and those for doubly-charged particles in Section 6. Finally, Section 7 summarises our conclusions.

2. Previous LHC Searches

There have been previous searches for long-lived particles (LLPs) at the LHC by the ATLAS [49, 50, 55, 56] and CMS [51, 53, 57, 58] Collaborations. These searches are based on observables related to ionization loss, dE/dx , displaced tracks, displaced vertices, delayed decays and timing information on slowly-moving massive particles. Most of these unusual events are associated with conventional final states involving photons, charged leptons, jets and missing transverse energy, E_T^{miss} . In some cases those final states occur as the decay products of LLPs, whilst in other cases they are produced in association with the LLPs. In all these searches, the p_T of charged leptons, photons or jets and E_T^{miss} were used to trigger the event selection.

The ATLAS and CMS collaborations classified their LLP searches into two broad classes: (i) heavy stable charged particles (HSCPs) (that may decay outside the detector) [49–51, 53, 55]

¹Detailed discussions on various theoretical models of long-lived stable particles and their signatures can be found in [1–3, 45–48].

and (ii) decaying LLPs [56–58]. In the first case, the HSCP gives rise to signatures that are very different from traditional prompt signatures. Singly-charged ($|Q| = e$) HSCPs typically travel with speeds $\beta = v/c < 1$, giving rise to an ionization loss (dE/dx) that is different from that of minimum-ionising SM particles. Due to their slower speeds, these particles would also take an anomalously long time-of-flight (ToF) to reach the muon chamber. Using the information on ionization loss and ToF, the ATLAS and CMS collaborations set lower limits on the masses of such HSCPs, mainly in the context of supersymmetry and its variants. The ATLAS collaboration used a dataset of 36.1 fb^{-1} collected during the 13 TeV runs to look for such exotic particles. No significant signal events were observed over the expected background, and 95% CL upper limits were set on the production cross-sections of long-lived R-hadrons, as well as pairs of staus and charginos. These upper limits can be translated into lower limits on the masses of a long-lived gluino, sbottom, stop, stau and chargino of 2000, 1250, 1340 and 1090 GeV, respectively [50].²

The ATLAS Collaboration also performed a dedicated search for the anomalous ionisation signal arising from the pair production of $SU(3)_C$ and $SU(2)_L$ singlet multi-charged ($|Q| = Ze$, $2 \leq Z \leq 7$) HSCPs with spin-1/2 in the mass range from 50 to 1400 GeV using an integrated luminosity of 36.1 fb^{-1} [52]. Non-observation of any significant deviation from the standard model background translates into 95% CL upper limits on the Drell-Yan pair production cross-section as a function of the charge of a lepton-like HSCP for several values of Z between 2 and 7. This upper limit on the pair production cross-section can be recast into 95% CL lower limits on the masses of lepton-like HSCPs for charges $|Q| = Ze : 2 \leq Z \leq 7$, ranging between 980 GeV and 1220 GeV for $Z = 2$ and $Z = 7$, respec-

²A shorter-lived coloured LSP could decay inside a detector after hadronization to form an R-hadron, e.g., a gluino hadron may decay into pair of SM quark jets and the lightest neutralino, χ_1^0 . Using the same data set, the ATLAS Collaboration set a lower mass limit of 1290 - 2060 GeV on the gluino, assuming pair production followed by such a decay with $m_{\chi_1^0} = 100 \text{ GeV}$ [49].

tively. The CMS Collaboration studied the pair production of $SU(3)_C$ and $SU(2)_L$ singlet singly-charged ($Z = 1$), multiply-charged ($Z > 1$) and fractionally-charged ($Z < 1$) spin-1/2 HSCPs produced via the Drell-Yan process during Run 1 of the LHC at $\sqrt{s} = 7$ and 8 TeV, with integrated luminosities of 5 fb^{-1} and 18.8 fb^{-1} respectively. The 95% CL lower limit on the masses are 480 ($Z = 2/3$), 574 ($Z = 1$), 685 ($Z = 2$), 796 ($Z = 5$), 781 ($Z = 6$), 757 ($Z = 7$) and 715 ($Z = 8$) GeV, respectively [53].

The CMS Collaboration also put 95% CL lower mass bounds on the gluino, stop and stau of 1610, 1040 and 490 GeV, respectively, from the production of HSCPs at the 13 TeV LHC run using a data sample from an integrated luminosity of 2.5 fb^{-1} . The corresponding mass limits on $|Q| = 1e$ ($2e$) lepton-like fermions of 550 (680) GeV were obtained by the CMS collaboration [51].³

3. The MoEDAL detector

The MoEDAL detector [7] is located at Point 8 of the LHC, around the interaction point in the Vertex Locator (VELO) cavern of the LHCb detector. MoEDAL is largely a passive LHC detector, and the subdetector system of principal relevance for this analysis is comprised of a large array (120 m^2) of Nuclear Track Detector (NTD) stacks composed of CR39 and Makrofol plastic surrounding the interaction region. MoEDAL also has paramagnetic trapping volumes (MMTs) that can capture highly-ionizing electrically- and magnetically-charged particles. The possible decays of trapped long-lived electrically-charged particles can be monitored at a remote facility, and magnetically-charged particles are mon-

³A dedicated search by the CMS Collaboration for an anomalous signal arising from disappearing charged tracks using the data collected in Run 2 during the 13 TeV run of the LHC, corresponding to an integrated luminosity of 140 fb^{-1} , set a 95% CL lower limit $m_{\chi_1^\pm} = 880$ (700) GeV for a purely wino LSP in the AMSB model [20, 21] for $\tau_{\chi_1^\pm} = 3$ (33) ns, respectively [58]. The CMS Collaboration used a similar signature and 35.9 fb^{-1} of data from the 13 TeV LHC run [59] to constrain the $SU(2)_L$ -triplet charged fermion mass m_{Σ^\pm} in the Type-III Seesaw model [24] to be $> 840 \text{ GeV}$.

itored at the ETH Zurich SQUID Magnetometer Facility. MoEDAL also incorporates an array of TimePix pixel devices that serves as a real-time system for monitoring highly-ionizing backgrounds in the cavern. We do not consider the MMTs and TimePix devices in this analysis, but focus on the capabilities of the NTD stacks.

The NTD elements of the MoEDAL detector are passive, not needing a trigger, electronic read-out, high-voltage or gas system. They are calibrated directly for highly-ionizing particles by using heavy-ion beams. Thus, they complement the main LHC detectors, ATLAS and CMS, which are not optimized for detecting heavily-ionizing particles. The NTD array has a low threshold and can detect particles with an ionization level $Z/\beta \sim 7$, where Z is the electric charge and β is the velocity of the particle. The charge resolution of the plastic NTDs is better than $0.05e$, where e is the electric charge. The TDR NTD array is supplemented by a Very High Charge Catcher (VHCC) subdetector with threshold $Z/\beta \sim 50$ applied directly to the outside of the VELO detector housing so as to increase the geometrical acceptance for magnetic monopoles, which does not play a role in our analysis.

After the NTD sheets are etched they must be scanned using optical microscopes, since the feature (etch-pit) sizes lie in the range 20 to 50 μm . A computer-controlled optical scanning microscope system will be deployed for MoEDAL data taking during Run 3. The system will be controlled by dedicated artificial intelligence (AI) software that is designed to recognize signal etch-pits in the presence of beam-induced backgrounds.

The multi-sheet structure of the NTD stack enables the measurements of individual pits to be combined to define a precise trajectory and effective Z/β values that measure the change in ionization energy loss as the particle loses energy during its passage through the NTD detector stack, demonstrating that the track comes from the interaction region and has dE/dx values consistent with a heavily-ionizing electrically-charged particle.

These characteristics of the NTD system ensure that such a particle can be detected with

high efficiency and confidence within the geometric acceptance of the detector.

4. Analysis framework

In this study we consider the pair production of singly- and doubly-charged particles at the LHC, $pp \rightarrow Y\bar{Y} + X$, where \bar{Y} represents the antiparticle of Y (which is same as Y if it is self-conjugate), and X represents soft particles originating from the beam remnants and initial- and final-state QCD radiation. The particle Y may be a supersymmetric particle, specifically an R-hadron containing the strongly-interacting $\tilde{g}, \tilde{q}, \tilde{t}$, a chargino $\tilde{\chi}^\pm$ or a charged slepton $\tilde{\ell}^\pm$, or a doubly-charged particle with spin-0, S^{++} , or spin-1/2, f^{++} .

As already discussed, the MoEDAL detector is insensitive to electrically-neutral particles and a coloured supersymmetric particle must be hadronized into a charged R-hadron to be detected. Since this probability κ (the charged vs neutral R-hadron fraction) is not well understood [60], we vary this parameter over the range $\kappa \in [0.5, 0.7]$. The distances between the interaction point and the MoEDAL's NTD panels are on average ~ 2 m, so MoEDAL is sensitive to particles Y with lifetimes τ longer than $\mathcal{O}(1)$ m/ c , otherwise the detection probability is exponentially suppressed. In this study we treat τ as a free parameter and in the next Section we identify the region of the mass vs lifetime plane for each choice of Y that can be probed by MoEDAL with Run 3 data.

As also discussed in the previous Section, the MoEDAL detector is essentially free of SM backgrounds, and we are therefore interested in the regions of parameter space where the numbers of expected signal events detected by MoEDAL are $N_{\text{sig}} \geq 1$ and 2, which we define as the thresholds for ‘‘evidence’’ and ‘‘discovery’’. The numbers of expected signal events are estimated by Monte Carlo simulation using the following formula:

$$N_{\text{sig}}(m, \tau) = \sigma(m) \cdot L \cdot \left\langle \sum_i \Theta(\beta_{\text{th}} - \beta_i) P(\vec{\beta}_i, \tau) \right\rangle_{\text{MC}}, \quad (1)$$

where $\sigma(m)$ is the production cross-section as a

function of the target particle's mass, m , L is the integrated luminosity, $\vec{\beta}$ is the particle's three-velocity, and $\langle \dots \rangle_{\text{MC}}$ represents the Monte Carlo average. The summation over i includes the two target particles Y and \bar{Y} in the event. The Heaviside step function ($\Theta(x) = 1$ for $x > 0$ and 0 otherwise) models the fact that the NTDs are capable to detect a particle with ionization level higher than some threshold, $Z/\beta > 1/\beta_{\text{th}}$.

The threshold velocity β_{th} for detection depends in principle on the incident angle between the direction of the particle and the NTD panel. This effect was significant in Run 2 of the LHC, because the NTD panels were not ideally oriented (see [8] for a study of this effect). However, in Run 3 all the NTD panels will be facing the interaction point and the incident angles are always close to optimal. We therefore use a constant threshold velocity β_{th} in this study for Run 3. We take $\beta_{\text{th}} = 0.15$ (0.3) for singly- (doubly-)charged particles.

We denote the probability for the target particle with three-velocity $\vec{\beta}$ and lifetime τ to survive and hit an NTD panel by $P(\vec{\beta}_i, \tau)$, which can be expressed as

$$P(\vec{\beta}, \tau) = \epsilon(\vec{\beta}) \cdot \exp\left(-\frac{l(\vec{\beta})}{\gamma\beta c\tau}\right). \quad (2)$$

In this expression $\epsilon(\vec{\beta}) = 1$ if there is an NTD panel in the direction of $\vec{\beta}$ and 0 otherwise. The exponential factor represents the probability that the target particle does not decay before reaching an NTD panel, where $l(\vec{\beta})$ is the distance between the interaction point and the NTD panel in the direction of $\vec{\beta}$, τ is the lifetime and $\gamma = (1 - \beta^2)^{-1/2}$.

In order to evaluate the Monte Carlo average in Eq. (1) we used `Madgraph5_aMC v-2.6.7` [61], and implemented several types of doubly-charged particles using `FeynRules 2` [62].

5. Singly-charged sparticles

5.1. Motivations for candidates

Candidates for the long-lived sparticle include the gluino, squarks, Winos and Higgsinos, and sleptons.

The gluino is not detectable directly, since it hadronizes very soon after production to form colour-neutral hadrons. The colour of the gluino may be neutralized by a gluon, forming a neutral hadron, or by a colour-octet quark pair. We focus on the latter possibility, assuming that the gluino-gluon state is heavier. We further assume that gluino/first-generation quark states $\tilde{g}u\bar{u}, \tilde{g}d\bar{d}, \tilde{g}u\bar{d}$ and $\tilde{g}u\bar{u}$ are the lightest. Depending on the details of superhadronic spectroscopy, the lightest of all the gluino/quark states may be neutral or charged. In the former case MoEDAL would not see a signal: we consider here the latter case.

We consider separately the possibilities that the long-lived sparticle is the lightest squark, which may be a partner of one of the 5 lightest quarks, or a stop. We assume that in the former case the differences between these squark masses would be relatively small, with the stops much heavier, whereas in the light stop case the other squarks would be much heavier. In both cases, we assume that the other squark species decay into the lightest one on a time scale $\ll \mathcal{O}(1)$ m/c. The resultant long-lived squark would also appear as a bound state, of which the lightest is expected to be that with a first-generation antiquark, e.g., $\tilde{u}\bar{u}$, $\tilde{d}\bar{d}$, $\tilde{u}\bar{d}$ or $\tilde{d}\bar{u}$ if the lightest squark is associated with the first generation. In the former two cases the lightest squark hadron would be neutral, and MoEDAL would not see a signal: we assume here one of the latter cases of a charged long-lived particle.

Another possibility is that the long-lived sparticle is some mixture of Wino, \tilde{W} , and Higgsino, \tilde{h} , and we consider the cases where one or the other component dominates production. Decays into the lightest \tilde{W}/\tilde{h} combination would again occur on a time scale $\ll \mathcal{O}(1)$ m/c, and this combination could be either neutral or charged: we consider the latter case here.

We consider finally the possibility that the long-lived sparticle is a charged slepton, $\tilde{\ell}$, and our results apply to any flavour of slepton, assuming that the other slepton flavours are much heavier. The lightest slepton might be the supersymmetric partner of either a left- or right-handed lepton, and we consider both possibilities here, making the conservative assumption that

the heavier one is heavy enough to be effectively decoupled. In what follows we refer to the lightest slepton as the $\tilde{\tau}_{L/R}$, since the tau slepton is the lightest in many supersymmetric models. However, it should be noted that the numerical results for $\tau_{L/R}$ are also applicable to the other sleptons, namely $\tilde{e}_{L/R}$ and $\tilde{\mu}_{L/R}$, as long as they are the lightest and other states are decoupled. We recall that the detection with MoEDAL of long-lived sleptons via the cascade decays of long-lived gluinos was studied in [8, 9], whereas in this Section we consider the direct pair production of long-lived sleptons.

5.2. Run 3 projections for supersymmetric particles

We begin the discussion of MoEDAL's projected sensitivity at Run 3 for singly-charged long-lived supersymmetric particles, showing in the upper panel of Fig. 1 the 13 TeV cross-sections for pair production of various supersymmetric particle species. The cross-sections are all taken from the LHC SUSY Cross Section Working Group [63], except for $\tilde{\tau}_L$, for which we used Resummino 2.0.1 [65]. The cross-sections for coloured supersymmetric particles (\tilde{g} , \tilde{q} and \tilde{t}_1) are computed including approximate next-to-next-to-leading order (NNLO_{Approx}) supersymmetric QCD corrections and the resummation of soft gluon emission at next-to-next-to-leading-logarithmic (NNLL) accuracy [64], whereas those for the weakly-interacting supersymmetric particles (\tilde{W} , \tilde{h} and $\tilde{\tau}_{L/R}$) are calculated to NLO+NLL accuracy.

The curve for \tilde{q} in the upper panel of Fig. 1 is the sum of the cross-sections for both the left- and right-handed versions of all 5 light-flavoured squarks, calculated assuming $m_{\tilde{g}} = 3$ TeV. In the cases of electroweakly-interacting sparticles, the cross-sections are summed over all triplet (doublet) components for \tilde{W} (\tilde{h} and $\tilde{\tau}_L$). Namely, we included $\tilde{W}^{\pm}\tilde{W}^0$ and $\tilde{W}^+\tilde{W}^-$ production for Winos, $\tilde{h}^+\tilde{h}^-$, $\tilde{h}_{1,2}^0\tilde{h}^{\pm}$ and $\tilde{h}_1^0\tilde{h}_2^0$ production for Higgsino and $\tilde{\tau}_L^+\tilde{\tau}_L^-$, $\tilde{\nu}_\tau\tilde{\tau}_L^{\pm}$ and $\tilde{\nu}_\tau\tilde{\nu}_\tau$ for producing the left-handed slepton, assuming that the heavier components of the multiplets decay promptly into the lightest charged partner, which we as-

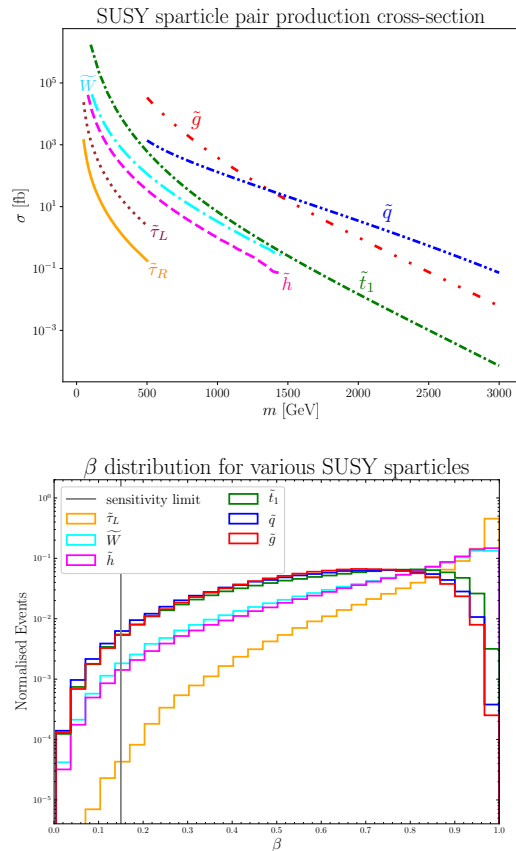


Figure 1. *Upper panel: the production cross-sections for various sparticle species. For the coloured particles (\tilde{g} , \tilde{q} and \tilde{t}_1), we show NNLO_{Approx}+NNLL cross-sections [63], while the cross-sections plotted for the weakly-interacting particles (\tilde{W} , \tilde{h} and $\tilde{\tau}_{L/R}$) are calculated to NLO+NLL accuracy [64]. Lower panel: the velocity distributions for various sparticle species. The following representative masses were chosen: \tilde{g} : 1010 GeV, \tilde{q} : 920 GeV, \tilde{t}_1 : 720 GeV, \tilde{W} : 300 GeV, $\tilde{\tau}_L$: 80 GeV.*

sume to be long-lived.⁴

As expected, one can see in Fig. 1 that the coloured sparticles have the largest cross-sections, while sleptons $\tilde{\tau}_{L/R}$ have smaller cross-sections. For cross-sections to be above 1 pb, the masses have to be smaller than around 1 TeV (\tilde{g}), 700 GeV (\tilde{q}, \tilde{t}_1), 400 GeV (\tilde{W}, \tilde{h}) and 200 GeV ($\tilde{\tau}_{L/R}$).

As already mentioned, the production velocity of a singly-charged particle must be $< \beta_{\text{th}} = 0.15$ for it to be detectable by MoEDAL’s NTDs. In the lower panel of Fig. 1 we show the normalised velocity distributions for various sparticle species, as computed with `MadGraph5_aMC`. We took the following representative masses for this purpose: \tilde{g} : 1010 GeV, \tilde{q} : 920 GeV, \tilde{t}_1 : 720 GeV, \tilde{W} : 300 GeV, $\tilde{\tau}_L$: 80 GeV. The velocity distribution of the right-handed slepton $\tilde{\tau}_R$ (not shown) is similar to that shown for the $\tilde{\tau}_L$.

We see that the coloured sparticles have, in general, much lower velocities than the weakly-interacting sparticles. One reason for this is that the masses used in this calculation are larger for coloured particles than for weakly-interacting ones, so their production is more central. Another effect is that the production of coloured particles may be dominated by the gluon-gluon-initiated t -channel process. On the other hand, the production of weakly-interacting particles is largely dominated by the Drell-Yan s -channel process from a quark-antiquark initial state. We also observe that the fermionic particles \tilde{W} and \tilde{h} , have much lower velocities than the scalar particle $\tilde{\tau}_L$ ($\tilde{\tau}_R$) on average. This is because the s -channel process is mediated by spin-1 gauge bosons ($\gamma/Z/W^\pm$), and the pair-production rate for scalar particles vanishes in the limit of $\beta \rightarrow 0$ because of p -wave suppression, which is absent for the pair production of the fermionic particles \tilde{W} and \tilde{h} .

The grey vertical line in the lower panel of Fig. 1 marks the detection threshold velocity $\beta_{\text{th}} = 0.15$, and the portions of the distributions to the left of this line can be detected. We see that

⁴ Charged Winos are usually heavier than the neutral one by an amount $> m_{\pi^\pm}$, due to radiative corrections. However, the mass ordering can be reversed by tuning the mixing in the chargino and neutralino sectors, which is the scenario considered in this study.

the detection efficiency is highest for coloured supersymmetric particles, much lower for the slepton, and intermediate for \tilde{W} and \tilde{h} .

We now discuss the expected sensitivities of MoEDAL to long-lived supersymmetric particles in Run 3 of the LHC, assuming an integrated luminosity of 30 fb^{-1} . In Fig. 2 we show the contours of $N_{\text{sig}} = 1$ (solid) and 2 (dashed), corresponding to the thresholds for “evidence” and “discovery”, respectively, for strongly-interacting sparticles in mass versus $c\tau$ planes. The top panel shows the sensitivities for gluinos with the red and blue contours corresponding to the charged R-hadron fractions of $\kappa = 0.5$ and 0.7 , respectively. Under the optimistic assumptions $\kappa = 0.7$ and $c\tau \gtrsim 100\text{m}$, MoEDAL is expected to see 1 (2) signal event(s) for $m_{\tilde{g}} \simeq 1600$ (1470) GeV, while in the more conservative case $\kappa = 0.5$, the mass reach is ~ 1530 (1400) GeV for $N_{\text{sig}} = 1$ (2).

The middle panel of Fig. 2 shows the MoEDAL sensitivity to light-flavour squarks. Since the production cross-section depends on $m_{\tilde{g}}$, we show results for two gluino masses, $m_{\tilde{g}} = 2$ TeV for $\kappa = 0.5$ (red) and $\kappa = 0.7$ (blue) and 3 TeV for $\kappa = 0.5$ (green) and $\kappa = 0.7$ (magenta). We see from the plot that the mass reach is greater for the smaller gluino mass, since the cross-section for light-flavour squark production is larger in this case. In the most optimistic case ($m_{\tilde{g}} = 2$ TeV, $\kappa = 0.7$, $c\tau \gtrsim 100\text{m}$), MoEDAL could detect the gluino up to ~ 1920 (1700) GeV for $N_{\text{sig}} = 1$ (2). On the other hand for $m_{\tilde{g}} = 3$ TeV and $\kappa = 0.5$, the mass reach is ~ 1670 (1450) GeV for $N_{\text{sig}} = 1$ (2).

The Run 3 sensitivity for the lighter stop, \tilde{t}_1 , is presented in the bottom panel of Fig. 2, where the convention for the line-styles is the same as in the top panel. We see that a long-lived \tilde{t}_1 could be probed by MoEDAL up to $m_{\tilde{t}_1} \sim 920$ ($N_{\text{sig}} = 1$) and 830 ($N_{\text{sig}} = 2$) GeV for $\kappa = 0.7$, while the reach is ~ 870 ($N_{\text{sig}} = 1$) and 780 ($N_{\text{sig}} = 2$) GeV for $\kappa = 0.5$.

We now turn to discuss the expected sensitivities for weakly-interacting sparticle species shown in Fig. 3. The Run 3 projections for MoEDAL searches for a long-lived Wino (blue) and Higgsino (red) are shown in the top panel. We see that MoEDAL could probe the Wino up to

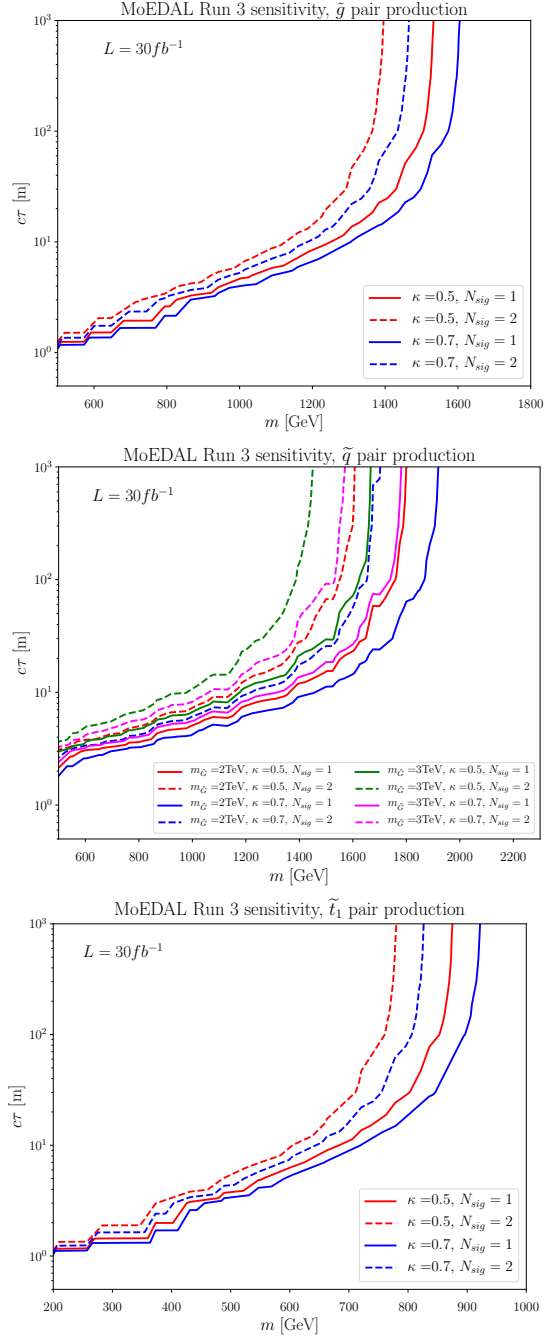


Figure 2. The expected sensitivities of MoEDAL for various long-lived strongly-interacting sparticle species, assuming 30 fb^{-1} of integrated luminosity. Top panel: the gluino, middle panel: squarks, bottom panel: the stop squark.

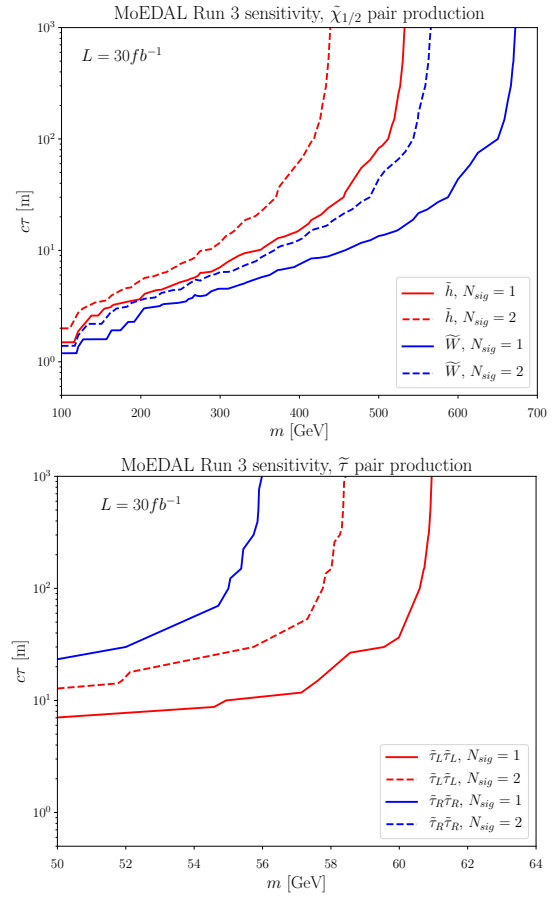


Figure 3. The expected sensitivities of MoEDAL for various long-lived electroweakly-interacting sparticle species, assuming 30 fb^{-1} of integrated luminosity. Upper panel: charginos, lower panel: sleptons.

$m_{\tilde{W}} \sim 670$ (570) GeV for $N_{\text{sig}} = 1$ (2) if $c\tau \gtrsim 100$ m, whereas the mass reach for the Higgsino with $c\tau \gtrsim 100$ m is $m_{\tilde{h}} \sim 530$ (430) GeV for $N_{\text{sig}} = 1$ (2). The higher mass reach for the Wino is obtained because the cross-section is larger thanks to its larger SU(2) charge.

The bottom panel of Fig. 3 shows the MoEDAL Run 3 sensitivities for long-lived sleptons, $\tilde{\tau}_R$ (blue) and $\tilde{\tau}_L$ (red). As can be seen, the mass reach is very low: it is 61 (58) GeV for the meta-stable $\tilde{\tau}_L$ with $N_{\text{sig}} = 1$ (2), and 56 GeV for $\tilde{\tau}_R$ with $N_{\text{sig}}=1$ (there is no corresponding contour for $N_{\text{sig}}=2$ for $\tilde{\tau}_R$). All of these reaches are below limits established at LEP [66] and already excluded. The reason for the low sensitivity is twofold. First, as discussed above the cross-sections for slepton production are very low, since production is mediated by spin-1 gauge bosons in the s -channel process and the production rate is velocity suppressed. Secondly, for the same reason the produced sleptons must have larger velocities than the other sparticle species examined here, as was also discussed previously. We conclude that, since MoEDAL targets highly-ionizing particles with $Z/\beta \gtrsim 7$, it is not sensitive to sleptons.

5.3. Comparison with the existing searches

We now compare the prospective MoEDAL sensitivities at Run 3 with the existing mass limits for metastable supersymmetric particles. Several different types of long-lived signatures have been discussed in the literature and searched for by ATLAS and CMS. For example, if gluinos have a lifetime of $1 - 100$ mm/ c and decay into dijets, they can be searched for by reconstructing the displaced vertices originating from metastable gluino decay [55, 57]. Another example is a disappearing track signature from long-lived winos with $\tau \sim 1 - 10$ cm/ c . The long-lived signature emerges when a charged wino is produced and decays into a nearly mass-degenerate neutral partner inside one of the silicon track detectors [56, 58]. Although the aforementioned searches are powerful for specific scenarios, they are not relevant for particles with longer lifetimes, or when the dominant decay modes differ from those assumed in the analyses. Since

	MoEDAL	(ATLAS)	(CMS)
\tilde{g}	1600	(2000)	(1500)
\tilde{q}	1920	((2310))	-
\tilde{t}	920	(1350)	(1000)
\tilde{W}	670	(1090)	-
\tilde{h}	530	((1170))	-
$\tilde{\tau}$	61	(430)	(230)

Table 1

Comparison between the MoEDAL mass reaches at Run 3 for $N_{\text{sig}} = 1$, $\kappa = 0.7$ and (in parentheses) the current (95% CL) mass bounds on several long-lived supersymmetric particle candidates obtained (estimated in the cases of \tilde{q} and \tilde{h} , in double parentheses) from the ATLAS heavy stable charged particle search with $L = 36.1$ fb $^{-1}$ [50] (second column) and CMS [51] (third column) under the model-dependent assumptions described there and in the text. All masses are in GeV.

the MoEDAL search is independent of the long-lived particle decay mode after passing through the NTDs, it avoids the model dependence of the above constraints.

There is, however, one type of search whose constraints are less model-dependent. These are heavy stable charged particle (HSCP) searches, which rely on large ionization energy loss dE/dx , the MoEDAL signature considered here, and time-of-flight (ToF) measurements, both of which are independent of the nature of decays.⁵ We therefore focus now on the constraints obtained from the HSCP searches.

In Table 1 we summarise the prospective MoEDAL mass reaches at Run 3 for $N_{\text{sig}} = 1$, $\kappa = 0.7$ and compare them with the current (95% CL) mass limits obtained by the most recent ATLAS HSCP analysis with $L = 36.1$ fb $^{-1}$ [50]. The ATLAS Collaboration interpreted their results for long-lived gluino, stop, Wino and stau candidates, and derived the lower bounds on their masses shown in parentheses in the third column of Table 1. At the time of writing, the most recent

⁵A scenario that can relax the constraint from HSCP analyses has been proposed and studied in [50].

CMS HSCP analysis [51] is based on a smaller set of data ($L = 2.5 \text{ fb}^{-1}$) and its limits on the gluino, stop and stau are weaker than those of ATLAS, as seen in the last column of Table 1.

The ATLAS constraints on the \tilde{g} , \tilde{t} and \widetilde{W} long-lived particle candidates are nominally stronger than the prospective reaches of MoEDAL with Run 3 data. However, the ATLAS selection cuts for this search may lead to gaps in the full phase space coverage that can be avoided by MoEDAL. As summarised in Table 1 of [50], ATLAS defined 5 signal regions (SRs), all of which incorporated E_T^{miss} triggers (varying between 70 and 110 GeV) or single (isolated) high-momentum muons.⁶ Depending on the scenario for long-lived sparticles that is considered, either or both of these auxiliary signatures may be absent. For example, there would be no E_T^{miss} signature in a scenario with weak R-parity violation, so these events would need to get selected by a muon-like signature in the detector.

We note also that in [50] ATLAS did not interpret their result in scenarios with long-lived light-flavour squarks or Higgsinos. In order to estimate the possible ATLAS mass reaches for these particles, we recast the cross-section upper limits for sbottoms (Winos) derived by ATLAS [50]. Our recasting assumes that the detection efficiencies of the HSCP analysis would be similar for light-flavour squarks and bottom squarks, and for Winos and Higgsinos. Based on this assumption we derive the mass bounds 2310 (1170) GeV for squarks (Higgsinos) shown in double parentheses in Table 1.

Comparing the prospective sensitivities of MoEDAL for long-lived sparticles with those of ATLAS and CMS, we note the following two points. One is that the luminosity to be accumulated by MoEDAL is only about one fifth of that already accumulated by ATLAS or CMS. This is because MoEDAL is located at Point 8 of the LHC together with the LHCb detector, which requires a restricted instantaneous luminosity so as to suppress pile-up.⁷ Secondly, MoEDAL is sen-

sitive only to particles with the ionization levels higher than $Z/\beta \gtrsim 7$, which reduces the acceptance for singly-charged HSCPs, in particular.

Finally, we comment on the case of an $SU(2)_L$ -triplet fermion, (Σ^\pm, Σ^0) , in a Type-III seesaw model, as was briefly mentioned in Section 1. In general, the mass degeneracy between Σ^\pm and Σ^0 is resolved due to radiative corrections in such a way $m_{\Sigma^\pm} - m_{\Sigma^0} > m_\pi^\pm$, which makes the lifetime of Σ^\pm too short for an HSCP signal in MoEDAL. However, if there are additional contributions to the mass splitting so that $m_{\Sigma^\pm} - m_{\Sigma^0} < m_\pi^\pm$, the lifetime of Σ^\pm would be long enough for detection of Σ^\pm at MoEDAL to be possible. For $m_{\Sigma^0} > m_{\Sigma^\pm} + m_\pi^\pm$, Σ^0 decays promptly to Σ^\pm and the mass reach would be ~ 670 GeV and the same as that for the Winos studied in this Section. For $m_{\Sigma^0} + m_\pi^\pm > m_{\Sigma^\pm} > m_{\Sigma^0}$, Σ^\pm undergoes three-body decay to Σ^0 with a lifetime $\mathcal{O}(10^{-6})$ s. In this case, the Σ^0 does not contribute to the signal and the signal yield would be reduced by roughly 1/2, since the dominant production mode is $pp \rightarrow \Sigma^\pm \Sigma^0$. We expect that the mass reach in this case would be similar to that for the Higgsino studied in this Section.

6. Doubly-charged particles

6.1. Motivations for candidates

Doubly-charged scalars can arise in variety of scenarios for physics beyond the standard model (BSM). As mentioned in Section 1, the Type-II seesaw model can provide doubly-charged scalars ($H^{\pm\pm}$) [29–34] that will be relevant for this analysis. In addition to the Type-II seesaw model, several other BSM scenarios, namely the Left-Right model [67–69], the Georgi-Machacek (GM) model [70–74], the 3-3-1 model [75,76] and the little Higgs model [77] also predict doubly-charged scalars. The supersymmetric versions of these models can lead to doubly-charged spin-1/2 Higgsinos. The minimal left-right supersymmetric model which is based on $SU(3)_C \times SU(2)_L \times SU(2)_R \times U(1)_{B-L}$ is one such model [38–42]. In addition to these particular well-studied models for multiply-charged scalars and fermions, such particles can also arise in the simplified models discussed in [43,44].

⁶Similarly, the CMS analysis [51] incorporates an $E_T^{\text{miss}} > 170$ GeV requirement.

⁷On the positive side, this restriction results in lower beam-related background in the MoEDAL NTD detectors.

In the pure Type-II seesaw model, the doubly-charged scalars ($H^{\pm\pm}$) belonging to the $SU(2)_L$ -triplet scalar multiplet Δ couple to leptons and the W boson, and the corresponding interaction strengths are controlled by the vacuum expectation value (v_T) of the neutral component of the Δ . This vev is related to the Majorana masses of the neutrinos: $M_\nu = \sqrt{2}Y_\nu v_T$, where Y_ν denotes the neutrino Yukawa couplings, and the collider limits on the mass of the doubly-charged scalars depend on the value of v_T . For small $v_T \leq 10^{-4}$ GeV that corresponds to large Y_ν , and assuming degenerate heavy scalar ($A, H, H^\pm, H^{\pm\pm}$) masses, $\text{Br}(H^{\pm\pm} \rightarrow \ell^\pm \ell^\pm) \approx 100\%$ ($\ell = e, \mu$). Using the like-sign dilepton (LSD) final state, the current lower bound on $m_{H^{\pm\pm}}$ varies between 770 GeV and 870 GeV [78] at the 95% CL from the direct search for a doubly-charged Higgs boson in the 13 TeV LHC run. The corresponding lower limit on $m_{H^{\pm\pm}}$ changes significantly for $v_T \geq 10^{-4}$ GeV (small Y_ν), when the LSD decay mode of $H^{\pm\pm}$ is highly suppressed while several competing decay modes of $H^{\pm\pm}$ start opening up, such as (i) a pair of heavy bosons $W^\pm W^\pm$, (ii) $W^\pm H^\pm$ and (iii) $H^\pm H^\pm$, if these are kinematically accessible. The subsequent decays of W and H^\pm into various leptons and jets give rise to rather complicated final states. Due to the cascade nature of the final state, the collider bound on the doubly-charged scalar is rather weak in this case.

The ATLAS collaboration studied the pair production of doubly-charged scalars that subsequently decay into pairs of W bosons (assuming $\text{Br}(H^{\pm\pm} \rightarrow W^\pm W^\pm) \approx 100\%$) in the 13 TeV LHC run. Non-observation of any signal beyond the standard model background sets a new limit on the doubly-charged scalar mass. Using a data sample from an integrated luminosity of 36.1 fb^{-1} , the $m_{H^{\pm\pm}}$ has been excluded between 200-220 GeV at 95% CL [79].

The left-right (LR) symmetric model predicts two types of doubly-charged scalars $H_L^{\pm\pm}$ and $H_R^{\pm\pm}$, corresponding to $SU(2)_L$ and $SU(2)_R$ triplet scalars Δ_L and Δ_R , respectively. As these two scalars belong to different gauge group, their couplings with fermions and gauge bosons are distinctly different. This is reflected in their produc-

tion rates at the LHC: $\sigma(pp \rightarrow H_L^{++} H_L^{--} + \dots) \approx 2.3 \times \sigma(pp \rightarrow H_R^{++} H_R^{--} + \dots)$, due to the different coupling strength of $H_{L,R}^{\pm\pm}$ with the Z boson [78, 80]. The ATLAS Collaboration looked for doubly-charged scalars in the LSD invariant mass distributions for the $e^\pm e^\pm$, $\mu^\pm \mu^\pm$ and $e^\pm \mu^\pm$ final states, and also in final states with three or four leptons (only electrons and muons) in the 13 TeV LHC run with an integrated luminosity of 36.1 fb^{-1} . No significant excess over the standard model prediction was observed. As a result, lower mass limits were obtained for the $m_{H_L^{\pm\pm}}$ and $m_{H_R^{\pm\pm}}$, assuming $\text{Br}(H_{L,R}^{\pm\pm} \rightarrow \ell^\pm \ell^\pm) = 100\%$ ($\ell = e, \mu$). The limit for $m_{H_L^{\pm\pm}}$ is same as that in the Type-II seesaw model. However, for the $m_{H_R^{\pm\pm}}$ the observed lower limit varies between 660 GeV and 760 GeV at the 95% CL [78].

In the GM model, the current LHC limit on $m_{H^{\pm\pm}}$ varies between 200 and 220 GeV at 95% CL, as obtained using an integrated luminosity of 36.1 fb^{-1} in the 13 TeV LHC run by the ATLAS Collaboration [79].

One should note that in all these search analyses only prompt decays of $H_{L,R}^{\pm\pm}$ scalars ($c\tau < 10\mu\text{m}$) were considered [78]. Hence they are complementary to the long-lived particle search that is possible with MoEDAL. In the Type-II seesaw model, there are certain regions of the $(v_T, m_{H^{\pm\pm}})$ parameter plane where the life-time of the doubly-charged scalar can be much longer. If the $H^{\pm\pm}$ were to decay outside an LHC detector, it would leave a heavily-ionizing charged track signal. Both the ATLAS and CMS collaborations have studied these signatures of such heavy long-lived particles, as we discuss later.

6.2. Run 3 projections for doubly-charged particles

We study here the prospective MoEDAL sensitivities to four types of doubly-charged particles: (singlet, triplet) \times (scalar, fermion). For the singlet and triplet types, the weak gauge quantum number assignments are $(SU(2)_L, U(1)_Y) = (\mathbf{1}, 2)$ and $(\mathbf{3}, 1)$, respectively, and all these particles are assumed to be colour singlets.

We show in the top panel of Fig. 4 the 13 TeV cross-sections for the production of doubly-

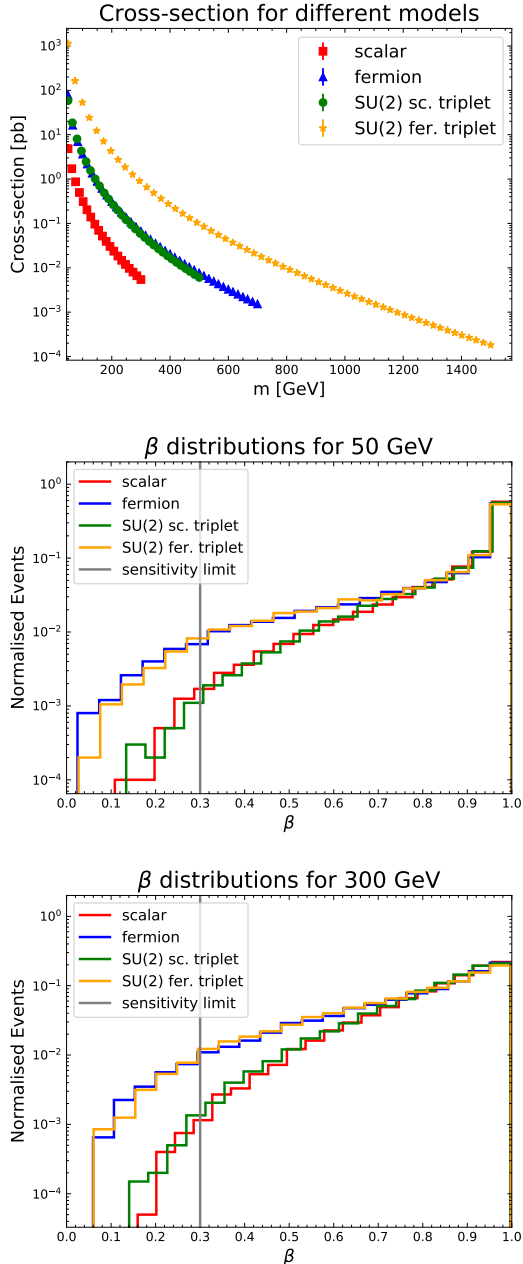


Figure 4. *Top panel: the leading-order production cross-sections at 13 TeV for various types of doubly-charged particles. Middle and lower panels: the velocity distributions for various doubly-charged particles with masses 50 and 300 GeV.*

charged particles. We see that, for species with the same spin, the cross-sections for triplet particles are an order of magnitude larger than those for the singlet. This is because we included all the neutral $pp \rightarrow Y^0 Y^0, Y^+ Y^-, Y^{++} Y^{--} + \dots$ and charged $pp \rightarrow Y^0 Y^\pm, Y^\pm Y^{\pm\pm} + \dots$ triplet production modes, assuming that the heavier components of the multiplets decay promptly into the nearly-degenerate lightest doubly-charged partner, so that all the production modes end up with the final state containing two doubly-charged particles. The neutral charge combinations are produced via s -channel γ/Z , while the charged ones are produced via an s -channel W^\pm . Unlike the triplet species, the singlet species has only one neutral production mode, namely $pp \rightarrow Y^{++} Y^{--} + \dots$.

We also see in the top panel of Fig. 4 that the cross-sections are an order of magnitude higher for fermions than scalars with the same gauge quantum numbers. One reason for this is that a Dirac fermion has twice as many degrees of freedom as a complex scalar. Another reason is, as already discussed in Section 5.2, the production of doubly-charged particles is mediated by s -channel gauge boson exchange, in which the two-scalar final states suffer threshold velocity suppression: $\sigma \rightarrow 0$ in the limit $\beta \rightarrow 0$. This suppression is absent for fermion pair production.

In the case of doubly-charged particles, the threshold velocity for detection is $\beta_{\text{th}} = 0.3$, higher by a factor of two compared to singly-charged ones due to the higher electric charge. In the middle and bottom panels of Fig. 4 we show the normalised velocity distributions for pair-produced doubly-charged particles with masses $m_Y = 50$ and 300 GeV, respectively. The grey vertical lines indicate $\beta_{\text{th}} = 0.3$, and only events to the left of the lines are detectable by MoEDAL. Comparing these two plots, we see that the distributions are more mass-dependent in the high- β region, whereas the mass effects are mild in the lower-velocity regions where $\beta \lesssim 0.3$. Nevertheless, about a factor of two more events satisfy $\beta < 0.3$ for $m_Y = 300$ GeV than for $m_Y = 50$ GeV. We also see clear differences in the momentum distributions between fermions and scalar particles for both $m_Y = 50$ and 300 GeV. As dis-

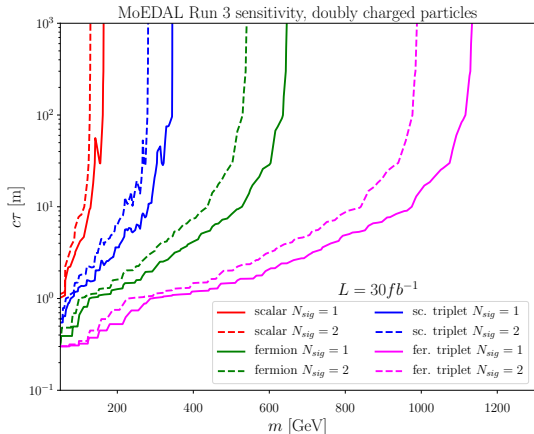


Figure 5. The expected sensitivities of MoEDAL for various long-lived doubly-charged particle species, assuming 30 fb^{-1} of integrated luminosity.

cussed earlier, this is because angular-momentum conservation again forces the scalar pair production via the s -channel gauge boson exchange to be velocity suppressed, $\sigma \rightarrow 0$ in the limit $\beta \rightarrow 0$. Unlike scalars, the production rate for fermions is non-vanishing even at $\beta = 0$.

We show in Fig. 5 the expected MoEDAL sensitivities for four types of colour-singlet doubly-charged particles: a scalar singlet (red), a scalar triplet (blue), a fermion singlet (green) and a fermion triplet (magenta), assuming a Run 3 integrated luminosity of 30 fb^{-1} . As expected from the above discussion, the fermion triplet has the highest mass reach among the four types, due to its large cross-section and favourable production velocities. MoEDAL can probe this particle up to $m_Y \sim 1130$ (990) GeV with $N_{\text{sig}} = 1$ (2) for the Run 3 luminosity if $c\tau \gtrsim 100 \text{ m}$, as indicated by the solid (dashed) line. The next most sensitive particle is the fermion-singlet, for which we estimate the MoEDAL mass reach with $c\tau \gtrsim 100 \text{ m}$ to be around 650 (540) GeV for $N_{\text{sig}} = 1$ (2). The mass reaches for the two scalar particles (singlet and triplet) are significantly lower than the corresponding fermionic particles, due to their smaller cross-sections and higher typical velocities. The MoEDAL mass reaches at Run 3 are around 340

	MoEDAL	(CMS)
Scalar singlet	160	((320))
Fermion singlet	650	(630)
Scalar triplet	340	((590))
Fermion triplet	1130	((900))

Table 2

Compilation of the prospective MoEDAL mass reaches ($N_{\text{sig}} = 1$) at Run 3 and comparison with the current (95% CL) mass bound for a long-lived fermion-singlet doubly-charged particle obtained from the CMS heavy stable charged particle search with $L = 2.5 \text{ fb}^{-1}$ [51] (in parentheses). Our estimates of possible CMS bounds on other types of particle are in double parentheses. All masses are in GeV.

(280) GeV for the scalar triplet and 160 (130) GeV for the scalar singlet for $N_{\text{sig}} = 1$ (2) if $c\tau \gtrsim 100 \text{ m}$.

6.3. Comparison with the existing searches

We compare prospective MoEDAL mass reaches ($N_{\text{sig}} = 1$) at Run 3 for the types of doubly-charged meta-stable particles examined in this Section, together with the available mass bound. As discussed in Section 5.3, the most relevant constraints are obtained by the heavy stable charged particle (HSCP) searches by ATLAS and CMS, which are based on the ionization energy loss dE/dx and the time-of-flight measurements but incorporate additional trigger requirements. The analysis utilizing the largest data-set ($L = 36.1 \text{ fb}^{-1}$) is that from ATLAS [50]. In Section 5.3 we compared the MoEDAL mass reaches for various long-lived sparticles with mass bounds from this analysis. However, ATLAS did not interpret their results for doubly-charged particles in [50], and did not provide mass limits.

CMS, on the other hand, has published their latest HSCP analysis [51] based on a smaller data-set, $L = 2.5 \text{ fb}^{-1}$, and have interpreted their result for a long-lived doubly-charged particle that is an SU(2) singlet and has spin-1/2. The mass bound for this particle is found to be 630 GeV, which is 20 GeV lower than the MoEDAL Run 3 mass reach, as shown in parentheses in Table 2.

We emphasize that the CMS analysis incorporated extra assumptions, such as an $E_T^{\text{miss}} > 170$ GeV requirement or the presence of a muon-like particle, rendering the result more model-dependent than the prospective MoEDAL sensitivity.

In [51], CMS did not directly interpret their result for other types of doubly-charged particles. In order to derive approximate mass bounds for other types of doubly-charged particles, we assume that the detection efficiencies are not very sensitive to the nature of particles other than the electric charge. With this assumption we use the cross-section upper limit for the fermion singlet particle provided in [51] as approximate cross-section limits for other types of doubly-charged particles (scalar singlet, scalar triplet and fermion triplet).

We estimate the CMS mass bound for scalar singlet (scalar triplet) obtained by the above recasting procedure to be ~ 320 (590) GeV, which can be compared with the corresponding MoEDAL mass reach of 160 (340) GeV ($N_{\text{sig}} = 1$, $L = 30 \text{ fb}^{-1}$). In the case of the fermion triplet, we estimate the CMS mass bound to be ~ 900 GeV, which is surpassed by the Run 3 mass reach of MoEDAL, which is 1130 GeV. Our estimates of these CMS sensitivities are shown in double parentheses, in view of potential model dependence associated with the CMS analysis assumptions and the fact that they are not official CMS results and have uncertainties due to our recasting procedure.

7. Conclusions

We have analysed in this paper the prospective sensitivities of the MoEDAL detector for searches for singly- and doubly-charged long-lived particles during Run 3 of the LHC, considering the specific examples of supersymmetric particles and scalars and fermions that are suggested by Type-II and Type-III seesaw models of neutrino masses, respectively. We emphasise that the MoEDAL search would be completely model-independent, using simply the capabilities of its NTDs. However, MoEDAL suffers from two disadvantages with respect to the general-purpose LHC detectors, ATLAS and CMS. It is sensitive only to an

anomalous level of ionisation corresponding to velocities $\beta < 0.15$ for singly-charged particles and $\beta < 0.3$ for doubly-charged particles, and it is anticipated that MoEDAL may accumulate 30 fb^{-1} of luminosity by the end of Run 3, an order of magnitude less than ATLAS and CMS.

The greatest MoEDAL sensitivities for supersymmetric particles are for strongly-interacting species, namely light-flavoured squarks, the gluino and stop squarks. There are also interesting sensitivities for long-lived charginos, whereas the sensitivity for a long-lived slepton is below the model-independent limit already established by LEP. However, we regard the model-independent potential MoEDAL sensitivities to other sparticles as quite complementary to the limits set by ATLAS and CMS, and of particular interest in scenarios such as those with weakly-broken R-parity in which there is no E_T^{miss} .

Among the particles examined in this paper, the doubly-charged fermion triplet appears to be the most favourable for MoEDAL. Since it is doubly-charged, the threshold velocity is relaxed to $\beta = 0.3$, so MoEDAL accepts a larger fraction of signal events. Since it is a fermion, the particles are much more likely to be produced near threshold than would be a scalar. Finally, it is an SU(2)-triplet and has the largest cross section among the doubly-charged particles we have studied. Therefore, the typical mass scale that can be probed is higher than for the other electroweakly-interacting cases, corresponding to a lower typical production velocity. Although our study suggests that the MoEDAL can probe a substantial non-excluded region of the parameter space of the fermion-triplet doubly-charged particle, one must keep in mind that the estimated CMS limit is approximate and based on a much smaller data set than that obtained by the end of Run 2.

It is clear that by the end of Run 3 ATLAS and CMS are likely to be able to provide better constraints on all the long-lived charged particle candidates that we have considered here. However, we would like to emphasise that the MoEDAL analysis we have described here would be able to set limits that are independent of auxiliary signal assumptions.

Acknowledgements

The work of J.E. was supported by the UK STFC Grant ST/P000258/1 and by the Estonian Research Council via a Mobilitas Plus grant. D.K.G. would like to thank the High Energy, Cosmology and Astroparticle Physics Division of ICTP, Trieste for hospitality during while part of this work was started. The work of R.M. is partially supported by the National Science Centre, Poland, under research grants 2017/26/E/ST2/00135. The work of K.S. is partially supported by the National Science Centre, Poland, under research grants 2017/26/E/ST2/00135 and the Beethoven grants DEC-2016/23/G/ST2/04301. D.K.G would like to thank N. Ghosh and I. Saha for discussions.

REFERENCES

1. L. Lee, C. Ohm, A. Soffer and T. Yu, “Collider Searches for Long-Lived Particles Beyond the Standard Model,” *Prog. Part. Nucl. Phys.* **106**, 210-255 (2019) [[arXiv:1810.12602](#) [hep-ph]].
2. J. Alimena et al., “Searching for Long-Lived Particles beyond the Standard Model at the Large Hadron Collider,” [[arXiv:1903.04497](#) [hep-ex]].
3. D. Curtin et al., “Long-Lived Particles at the Energy Frontier: The MATHUSLA Physics Case,” *Rept. Prog. Phys.* **82**, no.11, 116201 (2019) [[arXiv:1806.07396](#) [hep-ph]].
4. B. Acharya et al. [MoEDAL Collaboration], “Search for magnetic monopoles with the MoEDAL prototype trapping detector in 8 TeV proton-proton collisions at the LHC,” *JHEP* **08** (2016), 067 [[arXiv:1604.06645](#) [hep-ex]];
“Search for Magnetic Monopoles with the MoEDAL Forward Trapping Detector in 13 TeV Proton-Proton Collisions at the LHC,” *Phys. Rev. Lett.* **118** (2017) no.6, 061801 [[arXiv:1611.06817](#) [hep-ex]];
“Search for magnetic monopoles with the MoEDAL forward trapping detector in 2.11 fb⁻¹ of 13 TeV proton-proton collisions at the LHC,” *Phys. Lett. B* **782** (2018), 510-516 [[arXiv:1712.09849](#) [hep-ex]];
“Magnetic Monopole Search with the Full MoEDAL Trapping Detector in 13 TeV pp Collisions Interpreted in Photon-Fusion and Drell-Yan Production,” *Phys. Rev. Lett.* **123** (2019) no.2, 021802 [[arXiv:1903.08491](#) [hep-ex]].
5. B. Acharya et al. [MoEDAL Collaboration], “First search for dyons with the full MoEDAL trapping detector in 13 TeV pp collisions,” [[arXiv:2002.00861](#) [hep-ex]].
6. G. Aad et al. [ATLAS Collaboration], “Search for magnetic monopoles in $\sqrt{s} = 7$ TeV *pp* collisions with the ATLAS detector,” *Phys. Rev. Lett.* **109** (2012), 261803 [[arXiv:1207.6411](#) [hep-ex]];
“Search for magnetic monopoles and stable particles with high electric charges in 8 TeV *pp* collisions with the ATLAS detector,” *Phys. Rev. D* **93** (2016) no.5, 052009 [[arXiv:1509.08059](#) [hep-ex]];
“Search for magnetic monopoles and stable particles with high electric charges in 8 TeV *pp* collisions with the ATLAS detector,” *Phys. Rev. D* **93** (2016) no.5, 052009 [[arXiv:1509.08059](#) [hep-ex]].
7. B. Acharya et al. [MoEDAL], “The Physics Programme Of The MoEDAL Experiment At The LHC,” *Int. J. Mod. Phys. A* **29** (2014), 1430050 [[arXiv:1405.7662](#) [hep-ph]].
8. D. Felea, J. Mamuzic, R. Maselek, N. Mavromatos, V. Mitsou, J. Pinfold, R. Ruiz de Austri, K. Sakurai, A. Santra and O. Vives, “Prospects for discovering supersymmetric long-lived particles with MoEDAL,” [[arXiv:2001.05980](#) [hep-ph]].
9. K. Sakurai, D. Felea, J. Mamuzic, N. Mavromatos, V. Mitsou, J. Pinfold, R. Ruiz de Austri, A. Santra and O. Vives, “SUSY discovery prospects with MoEDAL,” [[arXiv:1903.11022](#) [hep-ph]].
10. ATLAS Collaboration, <https://twiki.cern.ch/twiki/bin/view/AtlasPublic/SupersymmetryPublicResults>.
11. CMS Collaboration, <https://twiki.cern.ch/twiki/bin/view/CMSPublic/PhysicsResultsSUS>.
12. S. P. Martin, “A Supersymmetry primer,”

- Adv. Ser. Direct. High Energy Phys. **21**, 1 (2010) [Adv. Ser. Direct. High Energy Phys. **18**, 1 (1998)] [[hep-ph/9709356](#)].
13. H. E. Haber and G. L. Kane, “The Search for Supersymmetry: Probing Physics Beyond the Standard Model,” Phys. Rept. **117**, 75 (1985).
 14. Manuel Drees, Rohini Godbole, and Probir Roy, “Theory And Phenomenology Of Sparticles: An Account Of Four-dimensional $N=1$ Supersymmetry In High Energy Physics”, Published in: Hackensack, USA: World Scientific (2004) 555 p
 15. H. Baer and X. Tata, ‘Weak scale supersymmetry: From superfields to scattering events,’ Published in : Cambridge University Press (2006) 556 p
 16. R. Barbieri *et al.*, “R-parity violating supersymmetry,” Phys. Rept. **420**, 1 (2005) [[hep-ph/0406039](#)].
 17. K. Barry, P. W. Graham and S. Rajendran, “Displaced vertices from R -parity violation and baryogenesis,” Phys. Rev. D **89**, no. 5, 054003 (2014) [[arXiv:1310.3853](#) [hep-ph]].
 18. N. Arkani-Hamed and S. Dimopoulos, “Supersymmetric unification without low energy supersymmetry and signatures for fine-tuning at the LHC,” JHEP **0506**, 073 (2005) [[hep-th/0405159](#)].
 19. G. F. Giudice and A. Romanino, “Split supersymmetry,” Nucl. Phys. B **699**, 65 (2004) Erratum: [Nucl. Phys. B **706**, 487 (2005)] [[hep-ph/0406088](#)].
 20. L. Randall and R. Sundrum, “Out of this world supersymmetry breaking,” Nucl. Phys. B **557**, 79 (1999) [[hep-th/9810155](#)].
 21. G. F. Giudice, M. A. Luty, H. Murayama and R. Rattazzi, “Gaugino mass without singlets,” JHEP **9812**, 027 (1998) [[hep-ph/9810442](#)].
 22. G. F. Giudice and R. Rattazzi, “Theories with gauge mediated supersymmetry breaking,” Phys. Rept. **322**, 419 (1999) [[hep-ph/9801271](#)].
 23. G. R. Farrar and P. Fayet, “Phenomenology of the Production, Decay, and Detection of New Hadronic States Associated with Supersymmetry,” Phys. Lett. B **76**, 575-579 (1978)
 24. R. Foot, H. Lew, X. He and G. C. Joshi, “Seesaw Neutrino Masses Induced by a Triplet of Leptons,” Z. Phys. C **44**, 441 (1989)
 25. B. Bajc and G. Senjanovic, “Seesaw at LHC,” JHEP **08**, 014 (2007) [[arXiv:hep-ph/0612029](#) [hep-ph]].
 26. A. Arhrib, B. Bajc, D. K. Ghosh, T. Han, G. Huang, I. Puljak and G. Senjanovic, “Collider Signatures for Heavy Lepton Triplet in Type I+III Seesaw,” Phys. Rev. D **82**, 053004 (2010) [[arXiv:0904.2390](#) [hep-ph]].
 27. M. Cirelli, N. Fornengo and A. Strumia, “Minimal dark matter,” Nucl. Phys. B **753** (2006), 178-194 [[arXiv:hep-ph/0512090](#) [hep-ph]].
 28. S. Jana, N. Okada and D. Raut, “Displaced Vertex and Disappearing Track Signatures in type-III Seesaw,” [[arXiv:1911.09037](#) [hep-ph]].
 29. J. Schechter and J. W. F. Valle, “Neutrino Masses in $SU(2) \times U(1)$ Theories,” Phys. Rev. D **22**, 2227 (1980).
 30. M. Magg and C. Wetterich, “Neutrino Mass Problem and Gauge Hierarchy,” Phys. Lett. **94B**, 61 (1980).
 31. T. P. Cheng and L. F. Li, “Neutrino Masses, Mixings and Oscillations in $SU(2) \times U(1)$ Models of Electroweak Interactions,” Phys. Rev. D **22**, 2860 (1980).
 32. G. Lazarides, Q. Shafi and C. Wetterich, “Proton Lifetime and Fermion Masses in an $SO(10)$ Model,” Nucl. Phys. B **181**, 287 (1981).
 33. R. N. Mohapatra and G. Senjanovic, “Neutrino Masses and Mixings in Gauge Models with Spontaneous Parity Violation,” Phys. Rev. D **23**, 165 (1981).
 34. M. Lindner, M. Platscher and F. S. Queiroz, “A Call for New Physics : The Muon Anomalous Magnetic Moment and Lepton Flavor Violation,” Phys. Rept. **731**, 1 (2018), [[arXiv:1610.06587](#) [hep-ph]].
 35. A. Melfo, M. Nemevsek, F. Nesti, G. Senjanovic and Y. Zhang, “Type II Seesaw at LHC: The Roadmap,” Phys. Rev. D **85**, 055018 (2012) [[arXiv:1108.4416](#) [hep-ph]].
 36. P. Bhupal Dev, D. K. Ghosh, N. Okada and I. Saha, JHEP **03**, 150

- (2013) doi:10.1007/JHEP03(2013)150 [arXiv:1301.3453 [hep-ph]].
37. D. K. Ghosh, N. Ghosh, I. Saha and A. Shaw, Phys. Rev. D **97**, no.11, 115022 (2018) doi:10.1103/PhysRevD.97.115022 [arXiv:1711.06062 [hep-ph]].
 38. R. Kuchimanchi and R. Mohapatra, “No parity violation without R-parity violation,” Phys. Rev. D **48**, 4352-4360 (1993) [arXiv:hep-ph/9306290 [hep-ph]].
 39. K. Babu and R. N. Mohapatra, “Minimal Supersymmetric Left-Right Model,” Phys. Lett. B **668**, 404-409 (2008) [arXiv:0807.0481 [hep-ph]].
 40. R. Francis, M. Frank and C. S. Kalman, “Anomalous magnetic moment of the muon arising from the extensions of the supersymmetric standard model based on left-right symmetry,” Phys. Rev. D **43**, 2369-2385 (1991).
 41. K. Huitu, J. Maalampi and M. Raidal, “Slepton pair production in e^+e^- collision in supersymmetric left-right model,” Phys. Lett. B **328**, 60-66 (1994) [arXiv:hep-ph/9402219 [hep-ph]].
 42. M. Frank, D.K. Ghosh, K. Huitu, S. K. Rai, I. Saha and H. Waltari, “Left-right supersymmetry after the Higgs boson discovery,” Phys. Rev. D **90**, no.11, 115021 (2014) [arXiv:1408.2423 [hep-ph]].
 43. A. Delgado, C. Garcia Cely, T. Han and Z. Wang, “Phenomenology of a lepton triplet,” Phys. Rev. D **84**, 073007 (2011) and references therein.
 44. A. Alloul, M. Frank, B. Fuks and M. Rausch de Traubenberg, “Doubly-charged particles at the Large Hadron Collider,” Phys. Rev. D **88**, 075004 (2013) and references therein.
 45. P. Bhupal Dev and Y. Zhang, “Displaced vertex signatures of doubly charged scalars in the type-II seesaw and its left-right extensions,” JHEP **10**, 199 (2018) [arXiv:1808.00943 [hep-ph]].
 46. S. Antusch, O. Fischer, A. Hammad and C. Scherb, “Low scale type II seesaw: Present constraints and prospects for displaced vertex searches,” JHEP **02**, 157 (2019) [arXiv:1811.03476 [hep-ph]].
 47. S. Banerjee, B. Bhattacharjee, A. Goudelis, B. Herrmann, D. Sengupta and R. Sengupta, “Determining the lifetime of long-lived particles at the LHC,” [arXiv:1912.06669 [hep-ph]]; S. Jana, N. Okada and D. Raut, “Displaced Vertex and Disappearing Track Signatures in type-III Seesaw,” [arXiv:1911.09037 [hep-ph]].
 48. O. Bulekov, M. Y. Khlopov, A. Romanouk and Y. S. Smirnov, “Search for Double Charged Particles as Direct Test for Dark Atom Constituents,” Bled Workshops Phys. **18** (2017) no.2, 11-24 [arXiv:1711.10773 [hep-ph]].
 49. M. Aaboud *et al.* [ATLAS Collaboration], “Search for heavy charged long-lived particles in proton-proton collisions at $\sqrt{s} = 13$ TeV using an ionisation measurement with the ATLAS detector,” Phys. Lett. B **788**, 96 (2019) [arXiv:1808.04095 [hep-ex]].
 50. M. Aaboud *et al.* [ATLAS Collaboration], “Search for heavy charged long-lived particles in the ATLAS detector in 36.1 fb^{-1} of proton-proton collision data at $\sqrt{s} = 13$ TeV,” Phys. Rev. D **99** (2019) no.9, 092007 [arXiv:1902.01636 [hep-ex]].
 51. V. Khachatryan *et al.* [CMS Collaboration], “Search for long-lived charged particles in proton-proton collisions at $\sqrt{s} = 13$ TeV,” Phys. Rev. D **94** (2016) no.11, 112004 [arXiv:1609.08382 [hep-ex]].
 52. M. Aaboud *et al.* [ATLAS Collaboration], “Search for heavy long-lived multicharged particles in proton-proton collisions at $\sqrt{s} = 13$ TeV using the ATLAS detector,” Phys. Rev. D **99**, no. 5, 052003 (2019) [arXiv:1812.03673 [hep-ex]].
 53. S. Chatrchyan *et al.* [CMS Collaboration], “Searches for Long-Lived Charged Particles in pp Collisions at $\sqrt{s}=7$ and 8 TeV,” JHEP **1307**, 122 (2013) [arXiv:1305.0491 [hep-ex]].
 54. C. Biggio, E. Fernandez-Martinez, M. Filaci, J. Hernandez-Garcia and J. Lopez-Pavon, “Global Bounds on the Type-III Seesaw,” [arXiv:1911.11790 [hep-ph]].
 55. M. Aaboud *et al.* [ATLAS Collaboration], “Search for long-lived, massive particles in events with displaced vertices and missing

- transverse momentum in $\sqrt{s} = 13$ TeV pp collisions with the ATLAS detector,” Phys. Rev. D **97** (2018) no.5, 052012 [[arXiv:1710.04901](#) [hep-ex]].
56. M. Aaboud *et al.* [ATLAS Collaboration], “Search for long-lived charginos based on a disappearing-track signature in pp collisions at $\sqrt{s} = 13$ TeV with the ATLAS detector,” JHEP **1806** (2018) 022 [[arXiv:1712.02118](#) [hep-ex]].
 57. A. M. Sirunyan *et al.* [CMS Collaboration], “Search for long-lived particles with displaced vertices in multijet events in proton-proton collisions at $\sqrt{s} = 13$ TeV,” Phys. Rev. D **98** (2018) no.9, 092011 [[arXiv:1808.03078](#) [hep-ex]].
 58. A. M. Sirunyan *et al.* [CMS Collaboration], “Search for disappearing tracks in proton-proton collisions at $\sqrt{s} = 13$ TeV,” [[arXiv:2004.05153](#) [hep-ex]].
 59. A. M. Sirunyan *et al.* [CMS Collaboration], “Search for Evidence of the Type-III Seesaw Mechanism in Multilepton Final States in Proton-Proton Collisions at $\sqrt{s} = 13$ TeV,” Phys. Rev. Lett. **119**, no.22, 221802 (2017) [[arXiv:1708.07962](#) [hep-ex]].
 60. ATLAS Collaboration, “Generation and Simulation of R-Hadrons in the ATLAS Experiment,” ATLAS-CONF-2019-019.
 61. J. Alwall *et al.*, “The automated computation of tree-level and next-to-leading order differential cross sections, and their matching to parton shower simulations,” JHEP **1407** (2014) 079 [[arXiv:1405.0301](#) [hep-ph]].
 62. N. D. Christensen and C. Duhr, “FeynRules - Feynman rules made easy,” Comput. Phys. Commun. **180** (2009) 1614 [[arXiv:0806.4194](#) [hep-ph]].
 63. LHC SUSY Cross Section Working Group, <https://twiki.cern.ch/twiki/bin/view/LHCPhysics/SUSYCrossSections>.
 64. W. Beenakker, C. Borschensky, M. Krmer, A. Kulesza and E. Laenen, “NNLL-fast: predictions for coloured supersymmetric particle production at the LHC with threshold and Coulomb resummation,” JHEP **1612** (2016) 133 [[arXiv:1607.07741](#) [hep-ph]].
 65. B. Fuks, M. Klasen, D. R. Lamprea and M. Rothering, “Precision predictions for electroweak superpartner production at hadron colliders with Resummino,” Eur. Phys. J. C **73** (2013) 2480 [[arXiv:1304.0790](#) [hep-ph]].
 66. LEP2 SUSY Working Group, “Stable Heavy Charged Particles,” http://lepsusy.web.cern.ch/lepsusy/www/stable_summer02/stable_208.html
 67. J. C. Pati and A. Salam, “Lepton Number as the Fourth Color,” Phys. Rev. D **10**, 275 (1974) Erratum: [Phys. Rev. D **11**, 703 (1975)].
 68. R. N. Mohapatra and J. C. Pati, “Left-Right Gauge Symmetry and an Isoconjugate Model of CP Violation,” Phys. Rev. D **11**, 566 (1975),
 69. G. Senjanovic and R. N. Mohapatra, “Exact Left-Right Symmetry and Spontaneous Violation of Parity,” Phys. Rev. D **12**, 1502 (1975).
 70. H. Georgi and M. Machacek, “Doubly Charged Higgs Bosons,” Nucl. Phys. B **262**, 463 (1985).
 71. M. S. Chanowitz and M. Golden, “Higgs Boson Triplets With $M(W) = M(Z) \cos \theta_W$,” Phys. Lett. **165B**, 105 (1985).
 72. J. F. Gunion, R. Vega and J. Wudka, “Higgs triplets in the standard model,” Phys. Rev. D **42**, 1673 (1990).
 73. J. F. Gunion, R. Vega and J. Wudka, “Naturalness problems for $\rho = 1$ and other large one loop effects for a standard model Higgs sector containing triplet fields,” Phys. Rev. D **43**, 2322 (1991),
 74. A. Ismail, H. E. Logan and Y. Wu, “Updated constraints on the Georgi-Machacek model from LHC Run 2,” [[arXiv:2003.02272](#) [hep-ph]], and references therein.
 75. J. E. Cieza Montalvo, N. V. Cortez, J. Sa Borges and M. D. Tonasse, “Searching for doubly charged Higgs bosons at the LHC in a 3-3-1 model,” Nucl. Phys. B **756**, 1 (2006) Erratum: [Nucl. Phys. B **796**, 422 (2008)].
 76. A. Alves, E. Ramirez Barreto, A. G. Dias, C. A. de S.Pires, F. S. Queiroz and P. S. Rodrigues da Silva, “Probing 3-3-1 Models in Diphoton Higgs Boson Decay,” Phys. Rev. D **84**, 115004 (2011).

77. N. Arkani-Hamed, A. G. Cohen, E. Katz, A. E. Nelson, T. Gregoire and J. G. Wacker, “The Minimal moose for a little Higgs,” *JHEP* **0208**, 021 (2002),
78. M. Aaboud *et al.* [ATLAS Collaboration], “Search for doubly charged Higgs boson production in multi-lepton final states with the ATLAS detector using protonproton collisions at $\sqrt{s} = 13$ TeV,” *Eur. Phys. J. C* **78**, no. 3, 199 (2018) [[arXiv:1710.09748](https://arxiv.org/abs/1710.09748) [hep-ex]].
79. M. Aaboud *et al.* [ATLAS Collaboration], “Search for doubly charged scalar bosons decaying into same-sign W boson pairs with the ATLAS detector,” *Eur. Phys. J. C* **79**, no. 1, 58 (2019) [[arXiv:1808.01899](https://arxiv.org/abs/1808.01899) [hep-ex]].
80. K. Huitu, J. Maalampi, A. Pietila and M. Raidal, “Doubly charged Higgs at LHC,” *Nucl. Phys. B* **487**, 27 (1997).